Kancherla *et al.*
Journal of Engineering and Applied Science (2024) 71:147
https://doi.org/10.1186/s44147-024-00477-9

Journal of Engineering and Applied Science

RESEARCH Open Access

Solar energy EV charging system using integrated Zeta-Luo converter

Ananda Babu Kancherla[1*], N. Bhanu Prasad[1] and D. Ravi Kishore[2]

*Correspondence:
akancherla@giet.edu

[1] Department of Electrical & Electronics Engineering, GIET University Gunupur, Orissa, India
[2] Department of Electrical & Electronics Engineering, GIET Rajahmundry, Andhra Pradesh, India

Abstract

This paper focuses on a grid-incorporated solar electric vehicle (EV) charging station that maximizes the acceptance of EVs in agricultural areas and reduces the over-reliance on the grid of urban cities. Since photovoltaic (PV) systems are widely available and easy to install, they are an excellent choice for EV charging applications. Hence, the aim of this work is to combine PV and EV, in order to achieve the objectives of both decarbonized energy generation and transportation. A Modified Zeta Integrated Luo Converter (MZILC), which provides a large conversion range combined with lower voltage stress, is proposed intending to increase the voltage level of the PV system. Furthermore, the converter generates a stable output devoid of fluctuations with the usage of the Grey Wolf–Grasshopper Optimized Proportional Integral (GW-GOPI) controller. Electricity for BLDC motors is generated by PV power during the day and supplied by a single-phase grid at night. The efficiency of the suggested grid-connected PV-based EV charging station is examined in MATLAB environment.

Keywords: GW-GOPI controller, BLDC motor, PV system, MZILC, 1ϕGrid

Introduction

The future potential for environmental, technological, and economic growth makes the rapid development of EV manufacturing and production more fascinating [1]. The effect of carbon dioxide (CO_2) production from fossil fuels on climate change is currently one of the top concerns. The cost of battery banks as storage in automobile systems is another problem [2]. Nevertheless, in order to produce an improved and stabilized voltage output, DC-DC converters are required due to PV's minimum output voltage [3]. Due to significant conduction losses, the Boost converter may offer huge step-up voltage at high duty ratios at the expense of efficiency [4]. Buck-boost converters with step-up and step-down abilities are not suitable due to the inverted output polarity and discontinuous nature of their input current [5]. As opposed to buck-boost converters, a single-ended primary-inductance converter (SEPIC) has a continuous input current, voltage conversion ratios, non-inverted output, and a series capacitor separating the output from the input. Although SEPIC suffer from high input current ripples, they still have a number of advantages over other converters [6–9]. The MZILC is chosen here for its similarity to buck-boost converters in that it converts DC-DC voltages while operating

with low ripple voltage outputs, high efficiency, and high power density. An unregulated input-power supply can also be regulated by this converter.

The contribution of an appropriate controller is considered essential for improving the changing qualities of the converter, especially for distributing a steady and governed output. The PI controller is one of the most often deployed controllers [10]. By adjusting PI parameters, several metaheuristic optimization techniques including Grey Wolf Optimization (GWO), Particle Swarm Optimization (PSO), Genetic Algorithm (GA), and others are proposed [11–15]. However, these algorithms still suffer from problems such as overdue convergence and presence trapped in local optima. Thus, this research proposes a hybrid GW-GO optimization algorithm. Once the regulation technique has created an uninterrupted output voltage, the BLDC motor operates using it as well [16]. It is more effective for EV applications since it has a primary outcome, wide speed range, excellent speed-torque characteristics, and low maintenance needs. In this study, the speed of a BLDC motor is managed by a PI controller.

EV charging system combined with batteries and PV generation with optimized operating cost management is presented in [17]. A PV-fed EV battery charging station for assisting distribution networks has been proposed in [18, 19] as part of an effective energy-management strategy. A consistent power supply is going to help in reducing the HPV's impacts of interruption and unpredictability. However, when there are grid faults, the proposed approach is more complicated. The control system that is being proposed can use different energy sources very effectively and can charge EVs continuously and affordably [20]. However, in grid-linked mode, the outputs of these controllers become zero. For developing a powered by solar energy BLDC motor utilized in EV infrastructure, an intensified marine predator algorithm has been proposed in [21]. Electric vehicles built on the PV structure, lower running expenses. However, controlling the motor speed is ineffective. Grid incorporated PV-based EV designed in [22] with hybrid optimized PI controller architecture. The BLDC motor drive for electric vehicles that have been chosen offers good speed control, outstanding effectiveness, and minimal upkeep. Nonetheless, the significant input current ripple content reduces the supreme power extraction capacity of PV in a broader range of values. Henceforth, this work proposes a PV-fed EV charring system using a hybrid GW-GO optimized PI controller. The primary contribution of this work is as follows,

- ➢ The combined EV and PV system is able to assist the grid through periods of high demand.
- ➢ By the employment modified zeta-integrated luo converter, the DC output voltage of the PV panel is enlarged.
- ➢ The working functionality of the proposed MZILC converter is enhanced through the use of a GW-GO-optimized PI controller.
- ➢ Using a PI/FLC/ANN controller guarantees that the BLDC motor is properly regulated in terms of speed.

Finally, the constant and distortion-free power is supplied to the BLDC motor. To assess the viability of the developed PV-based EV system, simulation results from MATLAB are utilized. The design of this article is as outlined below: the paper's "Proposed

system description" and "Modelling of proposed system" sections provide a description of the proposed system. The modeling of an acceptable converter and control system is covered in the "Modelling of proposed system" section along with a thorough controller design. The findings of the simulation are presented in the "Results and discussion" section. The paper's overall accomplishments are discussed in the "Conclusions" section.

Methods

Aim of the study

The aim of this study is to design and evaluate a grid-connected solar EV charging station that serves a dual purpose: to maximize EV adoption in agricultural areas and reduce the grid's burden in urban cities. The primary goal is to combine PV solar energy and EV charging, achieving both decarbonized energy generation and sustainable transportation. This research seeks to develop an innovative solution that addresses the energy needs of electric vehicles while harnessing the benefits of renewable solar power in a grid-connected setting.

Setting of the study

The study is conducted in a grid-connected environment, focusing on the integration of solar EV charging technology. The setting involves both rural agricultural areas and urban cities. It aims to address the unique challenges and requirements of these diverse settings. The study employs simulation and analysis tools, such as MATLAB, to evaluate the efficiency and feasibility of the proposed grid-connected PV-based EV charging station.

Proposed system description

The EV charging station is suggested here to overcome the issues of greenhouse gas and carbon emissions. Figure 1 demonstrates the diagram for PV PV-based EV charging system.

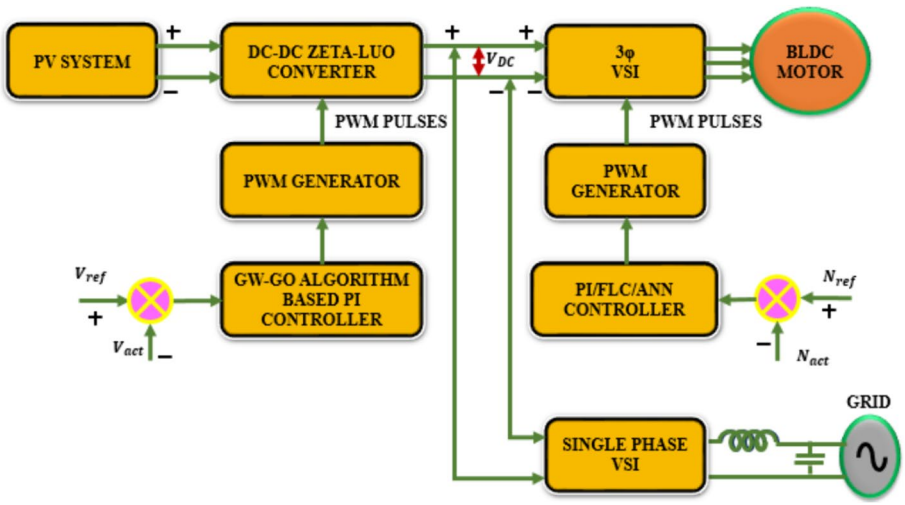

Fig. 1 PV-based EV charging system

The grid and PV system work together to power the BLDC motor. To gain the low output voltage that the PV system produces, MZILC is used in operation. The MZILC is improved with the deployment of a hybrid GW-GO PI controller. The ZILC actual output voltage is correlated to the reference voltage level, and the resultant error value is provided to the hybrid GW-GO optimized PI controller. By integrating the benefits of the two metaheuristic techniques used, the hybrid GW-GO algorithm efficiently aids in PI parameter weakening. Using an output from the controller, the PWM generator generates appropriate pulses to change MZILC's switching function. The BLDC motor of EV is derived by three-phase VSI, which obtains the stabilized voltage output from MZILC. The grid is used to power BLDC motors at night since solar power is unavailable. A single-phase VSI can also be used to feed excess power from the solar panels into the grid during the daytime. Using a PI/FLC/ANN controller guarantees that the BLDC motor is properly regulated in terms of speed.

Modelling of proposed system

A) Modelling of PV system

In a simulation scenario, a complete circuit replicates the I-V curve of a solar panel, which is normally made up of parallel strings of cells. N_s and N_p Fig. 2 indicates the PV cell circuitry diagram.

Moreover, the panel behavior can be calculated as

$$I_{PV} = N_P I_{ph} - N_p I_O \left\{ \exp\left[\frac{\left(V_{PV} + I_{PV} \times R_s \frac{N_s}{N_p} \right)}{N_s * \left(\frac{\eta k_b T}{q} \right)} \right] - 1 \right\} - \frac{V_{PV} + I_{PV} \times R_s \frac{N_s}{N_p}}{\frac{N_s}{N_p} R_{sh}} \tag{1}$$

In order to reduce the ripple voltage and regulate the output voltage from PV, the MZILC is connected.

B) Modelling of modified ZILC

Figure 3 illustrates the diagram for Modified ZLIC. PV electricity is generated, transmitted, and provided via precise control that modifies a modified ZILC's duty cycle in

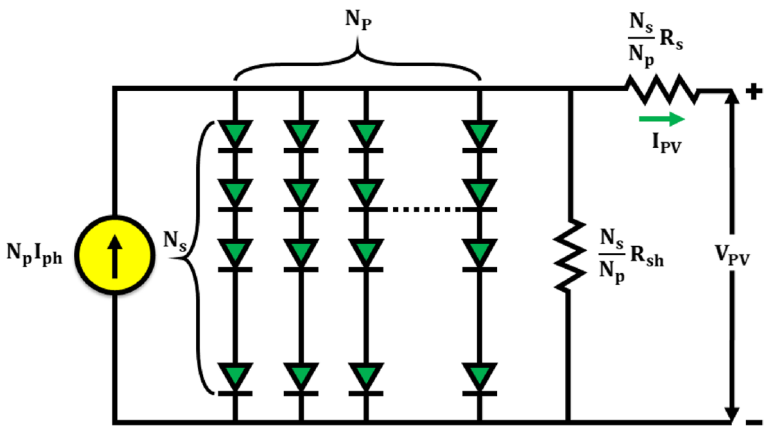

Fig. 2 Equivalent circuit for PV cell panel

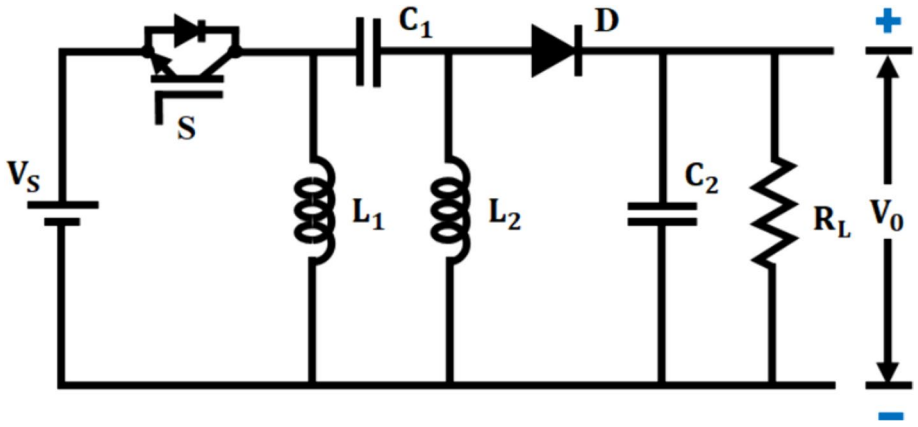

Fig. 3 Modified ZILC

response to quickly altering air conditions. Using a modified ZLIC converter as an interconnect, the solar panel and flexible load are connected.

Mode I

Figure 4a shows the corresponding circuitry for this mode. In this mode, the switch is turned on, inductors (L_1,L_2) and capacitor C_1 can store energy. I_{L1},I_{L2}, and V_{C_1} now have higher values. Furthermore, the diode is not in a charging phase, therefore the C_2's stored energy is lost to the load. The C_1 capacitor is initially negatively charged, increasing the voltage across it. When the diode's current drops to zero, the C_2 capacitor supplies the necessary power to the load.

Mode II

Figure 4b demonstrates the identical circuitry for this state. The switch is off in this mode. I_{L1} is rising while I_{L2} and V_{C_1} are beginning to decline as the capacitor C_1 starts to discharge. When the power switch is turned off in this mode of operation, the capacitor C_1 discharges and the current through L_1 rises. In contrast, the voltage across C_1 and the current flowing through the inductor I_{L2} have dropped. Through the conduction diode D, the capacitor C_2 begins to charge, and the sum of the two diode currents, I_{L1} and I_{L2}, forms the diode current. This process keeps going till V_{C_1}=V_{C_2}.

Mode III

Figure 4c shows the corresponding circuitry for this mode. In this mode, I_{L1} and I_{L2} are used to discharge the V_{C_1}<V_{C_2} and C_1. In this mode, I_{L2} discharges across the diode to charge C_2, resulting in a drop in I_{L2} and a rise in V_2. Once charging begins, the present I_{L1}, this mode of operation lasts until $I_{L2} = 0$.

Mode IV

Figure 4d depicts the corresponding circuitry for this mode. In this mode the inductor L_2<<L_1 operate in the discontinuous mode. For the duration of the switching period, the I_{L2} inductor discharges. L_1 has been increased and the C_1 has been released. In this mode, I_{L2} equals and opposes I_{L1}, and the diode is not conducting. Energy is lost by the

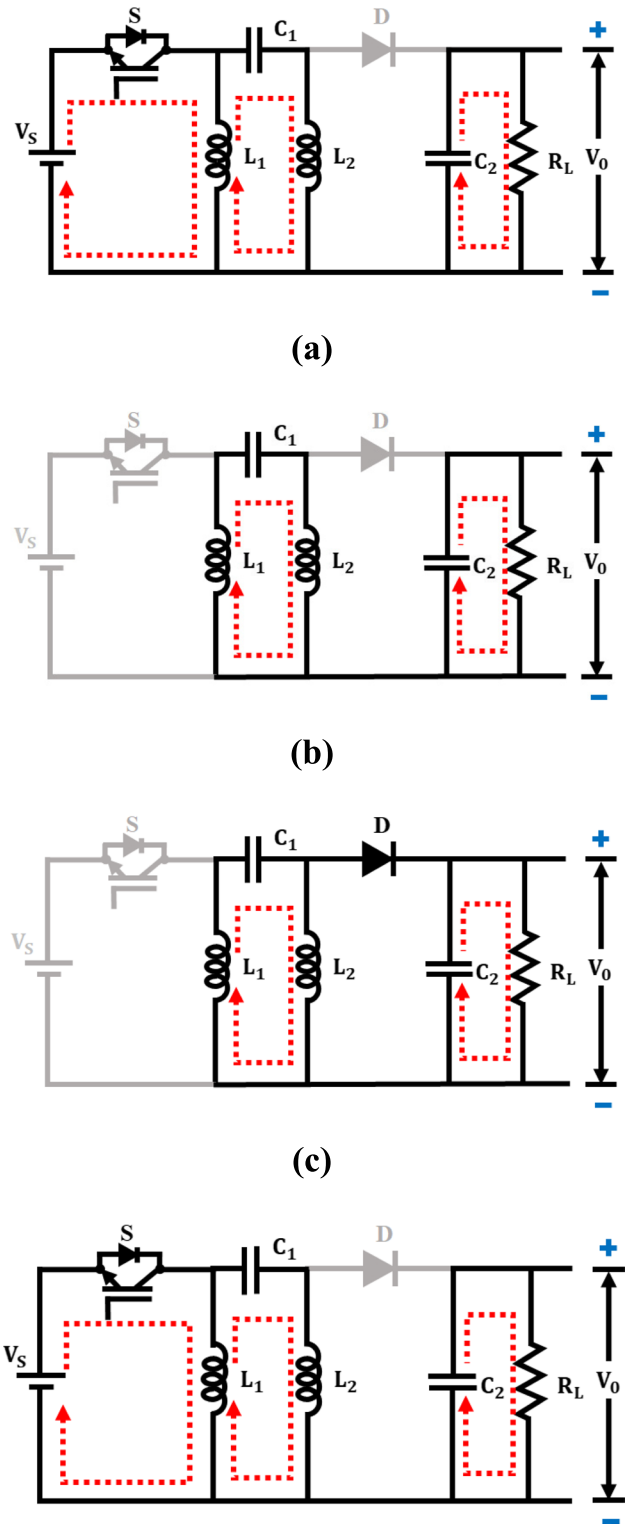

Fig. 4 Modes of operation **a** Mode I, **b** Mode II, **c** Mode III, **d** Mode IV

C_2 through the load, and V_{L_2} is decreased until $V_{C_1} = 0$. The output voltage V_{out} and L_1, L_2 is gets from [23] and the ZILC output voltage is

$$V_{\text{out}} = \frac{D_{\text{duty}}}{1 - D_{\text{duty}}} V_{PV} \tag{2}$$

Where D_{duty}—duty cycle of MZILC.

The capacitors (C_1,C_2) and inductors (L_1,L_2) are mathematically designed as

$$L_1 = \frac{V_{PV} D_{\text{duty}}}{\eta_e I_S F_{\text{switch}}} = \frac{R_{IN} D_{\text{duty}}}{\eta_e F_{\text{switch}}} = \frac{V_{PV}^2}{P_s} \frac{D_{\text{duty}}}{\eta_e F_{\text{switch}}} = \frac{1}{\eta_e F_{\text{switch}}} \times \frac{V_{PV}^2}{P_s} \times \frac{V_{\text{out}}}{V_{PV} + V_{\text{out}}} \tag{3}$$

$$L_2 = \frac{V_{out} \times 1 - D_{\text{duty}}}{2.I_{L2}.F_{\text{switch}}} = \frac{V_{\text{out}} D_{\text{duty}}}{2 I_{L1} F_{\text{switch}}} = \frac{R_{INV_{\text{out}}} D_{\text{duty}}}{2.V_{PV}.F_{\text{switch}}} = \frac{V_{PV}^2}{P_s} \times \frac{V_{\text{out}}}{2.V_{PV}.F_{\text{switch}}} \times \frac{V_{\text{out}}}{V_{PV} + V_{\text{out}}} \tag{4}$$

$$C_1 = \frac{V_{\text{out}} D_{\text{duty}}}{K_R.V_{C_1}.F_{\text{switch}}.R_{\text{Load}}} = \frac{V_{PV}}{K_R.F_{\text{switch}}.(V_{PV} + V_{out})^2} = \frac{V_{\text{out}} \times \frac{V_{\text{out}}}{(V_{PV} + V_{\text{out}})}}{K_R. \times V_{\text{out}} + V_{PV} \times F_{\text{switch}} \times (\frac{V_{\text{out}}^2}{P_s})} \tag{5}$$

$$C_2 = \frac{I_{C_1}}{2\omega_{\text{switch}}.V_{\text{out}}} = \frac{\frac{P_s}{V_{\text{out}}}}{2\omega_{\text{switch}} \delta_R V_{out}^2} \tag{6}$$

where, δ_R— ripple factor of the capacitor.

The conceptual demonstration of the proposed converter is illustrated in Fig. 5. The primary objective of this work is to optimize PI controller uniquely established to improve the controlling performance.

C) GW-GO Optimized PI controller

Hybrid GW-GO algorithm

A simple and effective hybrid model is implemented by the proposed GW-GO algorithm to enhance optimization capabilities without raising computational complexity. In order for a problem to be minimized, an individual's fitness function value must be lower than the average, which shows that the particle's nearby search region contains potential and promise. As a result, a method to improve local search should be used. On the other hand, it is impossible to employ a local search technique with a fitness function value higher than the average. Furthermore, the method does not prematurely converge with the addition of GO because the population becomes more randomly distributed as individual differences are scaled. Particularly during the last stages of evolution, this trait can better establish population diversity. Natural grasshoppers practice those main two operations in addition to searching for targets. To attain the accurate measurements, the numerical simulations are given by,

$$P_k = Q_k + L_k + B_k \tag{7}$$

Where P_k Dictates the position of the k_{th} grasshopper, Q_k is the social interaction, L_k is the gravity force and B_k defines the wind advection.

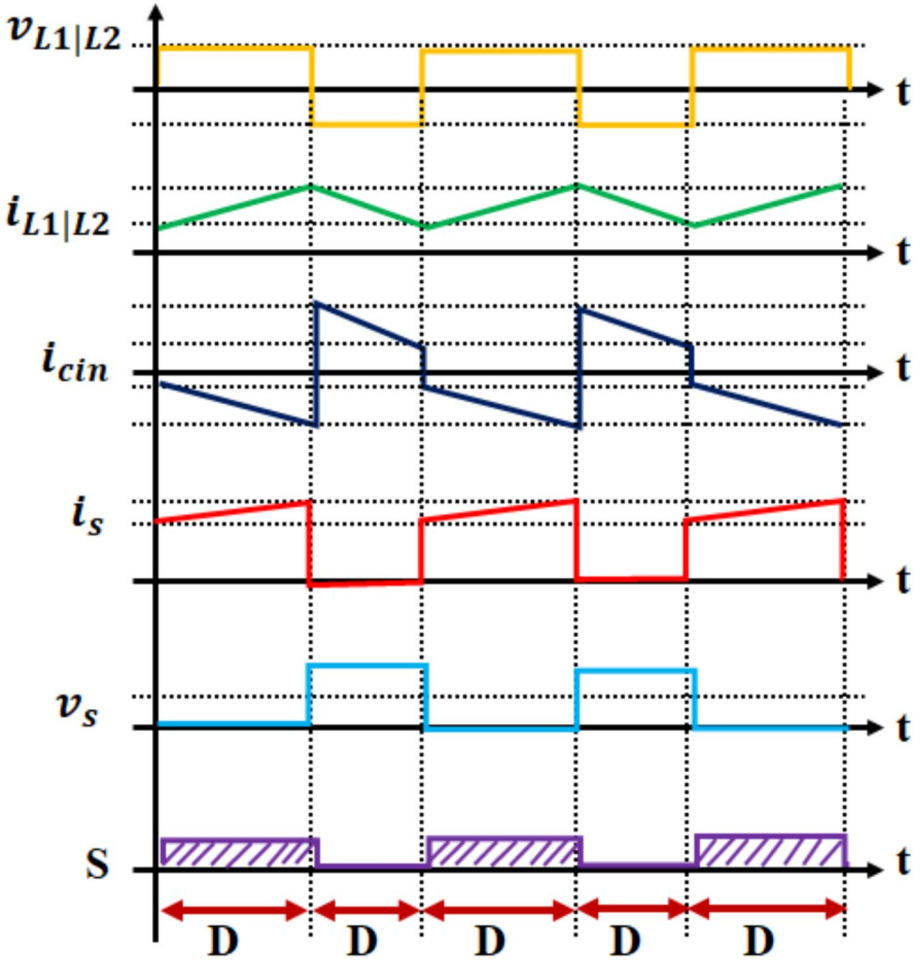

Fig. 5 Theoretical waveform of MZILC

The equation can be written as $P_k = rn_1 Q_k + rn_2 L_k + rn_3 B_k$, Then rn_1,rn_2 and rn_3 are random values in the range [0, 1], to produce random behavior.

$$Q_k = \sum_{\substack{l=1 \\ l \neq 1}}^{m} q(d_{k1}) d_{k1} \tag{8}$$

Where

d_{k1}—Distance between k_{th} and l_{th} grasshopper.

Algorithm 1 shows the hybrid GW-GO algorithm's code.

Algorithm 1. Hybridizing GW-GO

Input: initialize the population and GW-GO parameters;
Output: Optimal solution
Initialize the population of $P_k(k = 1,2,3, \ldots \ldots, n)$;
Initialize the parameters l, M and N;
Calculate the fitness of every search medium(wolf);
P_α=Global best solution search medium;
P_β=Local best solution search medium
While(r<M_{itera})
For single search medium
Normalize Grasshopper's distance;
Update Current position of search medium;
If (current search medium>boundary)
Retrieve current search medium;
End For
Update l value by equation.(10);
Update parameters M and N;
Calculate all search mediums fitness;
Update$P_\alpha$and P_β;
$r = r + 1$;
End while
Return a new values

The below Fig. 6 represents the Flow chart for the GW-GO Algorithm.

A specific heuristic enhances the prey to deliver the greatest possible outcome (i.e., an optimum values). According to the fitness function, the solution is assessed, and it

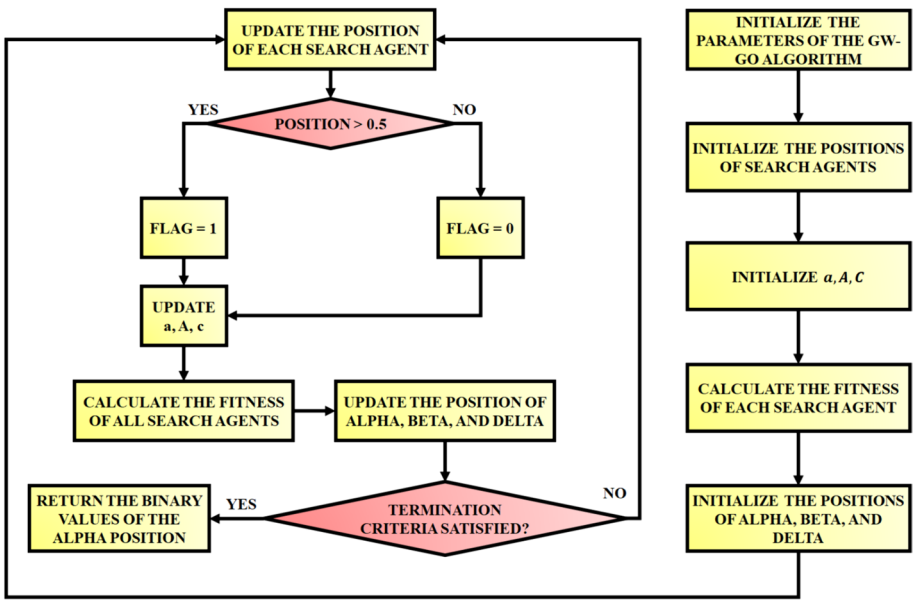

Fig. 6 Flow chart for GW-GO Algorithm

appears that every situation is a component of the space. The K_P and K_I values of PI controller, which regulates the switching behavior of the MZILC converter, are effectively tuned using the output from the GW-GO algorithm. Where the parameter values of the GW-GO optimized PI controller is $K_p = 0.2$ and $K_i = 0.1$.

D) BLDC motor speed control using PI/FLC/ANN controller

BLDC motor control has to know the rotor position and functioning to properly commutate the motor. Captured motor speed and/or motor current, as well as a PWM signal to modulate motor speed and power for closed-loop speed control are two further requirements. This work proposes a three controllers namely PI, FLC and ANN, when compared to the other two controllers the ANN regulates the motor speed efficiently. Figure 7 illustrates the basic flow of BLDC motor speed control.

PI controller

The BLDC motor's speed is managed by the PI controller, one of many extremely useful controllers for diverse applications. For the application of these controllers to produce the desired results, their modifying factors are a must. Therefore, it is imperative to employ a method that is both expedient and readily available. To ascertain these control variables ((*Kp*, *Ki*). The PI controller's control architecture is shown in Fig. 8.

Because of variations in operating points and shifts in system dynamics, PI controllers need to be returned frequently.

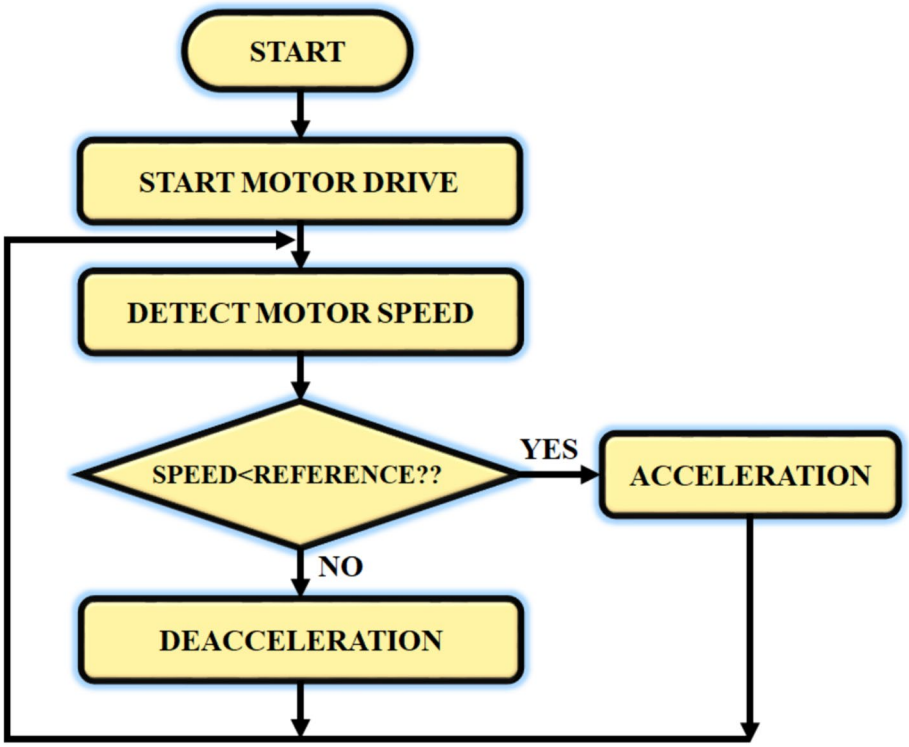

Fig. 7 Basic flow of BLDC motor speed control

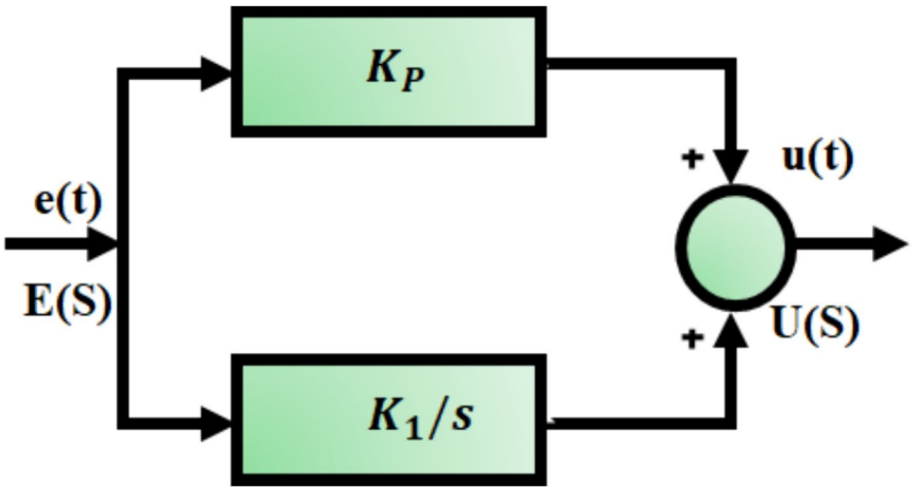

Fig. 8 Proposed PI controller

Fuzzy logic controller (FLC) A rule-driven controller is a fuzzy logic control or FLC. This algorithm seeks to account for human understanding to regulate a system without the need for a mathematical model. It relies on a linguistic control technique, rather than using variables with numbers, fuzzy logic utilizes linguistic variables. Fuzzification is the procedure of altering a numerical variable into a semantic variable. Here, the change in error (CE) and error (E) serve as the inputs for the fuzzy logic controller.

Calculation of speed error involves comparing the standard speed and real speed. The flexible control that the fuzzy logic controller generates allows the motor speed to precisely follow the reference speed. Defuzzification is the opposite of fuzzification, the FLCs are used to generate the necessary output in linguistic variables or fuzzy numbers. Based on the demands, semantic factors need to convert into crisp output. The level of involvement for each input is represented graphically by the membership function. Every input and output response has a particular membership function associated with it. For the output and input variables in this case, the trapezoidal membership functions are employed.

Artificial neural network (ANN) controller The precise position of the rotor within BLDC motors is detected by hall effect sensors. Depending on the rotor magnetic pole polarity, every hall effect sensor produces a High or Low signal providing information. In order to identify which switch gets supplied by the voltage source, the signal produced by the hall effect sensor is going to be delivered to inverter and then to commutation logic. The reference voltage produced by ANN is the voltage that enters the inverter as seen in Fig. 9.

With the help of a hybrid GW-GO optimized PI controller-based MZLIC converter, the voltage input of the 3 ϕ VSI is maintained constant. Through the use of pulses produced by a PWM generator, the output of the PI controller is used to regulate the 3 ϕ VSI's switching action. As a result, the PI controller efficiently regulates the

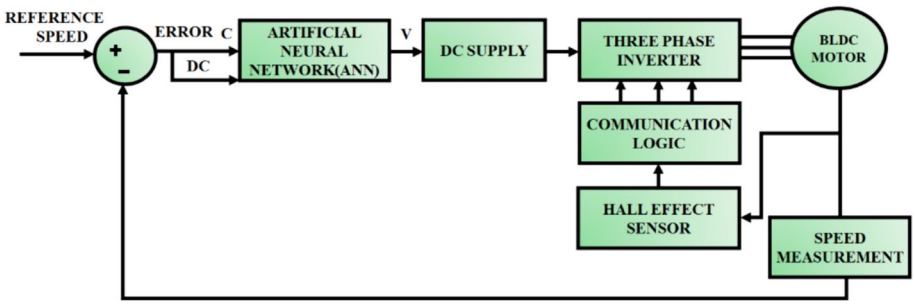

Fig. 9 Proposed ANN controller

Table 1 Parameter specification

Parameters	Ratings
Solar PV system	
Peak power	100 W, 15 panels
No. of cells connected in series	36
Open circuit voltage	22.68 V
Short circuit current	5.86 A
Modified Zeta-Luo converter	
C_1, C_2	$150\mu F$
L_1, L_2	$0.288mH$
Switching frequency	10 kHz

output frequency of the 3 ϕ VSI. Thus, the BLDC motor receives regulated and controlled voltage and frequency input, and speed control of the BLDC motor is ensured. An EV charging system is proposed that utilizes a single-phase to connect to the utility grid. An inverter's main job is to turn the DC electricity it receives into AC power so that it can supply the utility grid. By figuring out the voltage phase of the grid, it is feasible to synchronize the inverter output voltage and grid voltage phase.

Results and discussion

In order to increase the PV output of an EV-BLDC based on grid integrated PV, a novel ZETA integrated Luo converter is being used. In addition, GW-GO optimized PI controller is used to minimize steady-state errors and stabilize BLDC output. Table 1 summarizes the model's parameter specifications. Furthermore, MATLAB is used to test the proposed model and assess its performance using derived output.

The results examined using MATLAB Simulink for the proposed system design are as follows:

The waveform representation of PV voltage and current is illustrated in Fig. 10. Due to the intermittent nature of PV panels, the solar current and voltage get distorted initially. From Fig. 10a it is observed that voltage varies from 45 to 55 V and it gradually maintains the stable voltage value of 58 V after 0.2 s. Subsequently, with distortions at the beginning, a stabilized current of 13A is achieved after 0.2 s with minor fluctuations.

For the purpose of boosting the output voltage of the PV system with fewer switching losses, the MZILC is proposed here. The resultant current and voltage of the proposed

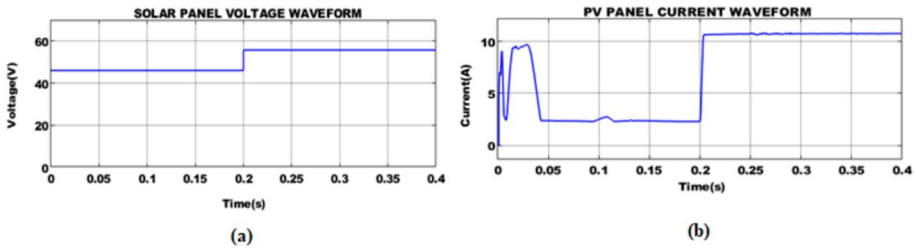

Fig. 10 Solar (**a**) voltage and (**b**) current waveforms

converter are illustrated in Fig. 11. From the evaluation is it clear that the stabilized voltage and current and value of 300 V and 2 A are attained respectively.

The waveforms of the grid's current and voltage are represented in Fig. 12 proving that the PI controller provides excellent grid synchronization. With magnitudes of 230 V for grid voltage and 10 A grid current, both of these waveforms are exactly sinusoidal and in phase.

The waveform representation of real and reactive power is demonstrated in Fig. 13. It is noted that a constant real power of 1000 W is obtained and the reactive power decreases and reaches a value nearer to zero.

This work establishes an efficient PI controller for controlling BLDC motors and the corresponding outputs of BLDC motors are shown in Fig. 14. It is detected that, with distortions at the beginning, a stable 4A motor current is achieved after 0.25 s and further maintained stable. Similarly, the back EMF of the motor is maintained stable till 0.2 s with 55 V, and after 0.25 s voltages get increased and sustained at 75 V further. The speed of the BLDC motor increases gradually and attains a maximum of 3000 rpm with variations at the starting stage. A 2N-M torque is achieved after 0.25 s with variations in the beginning.

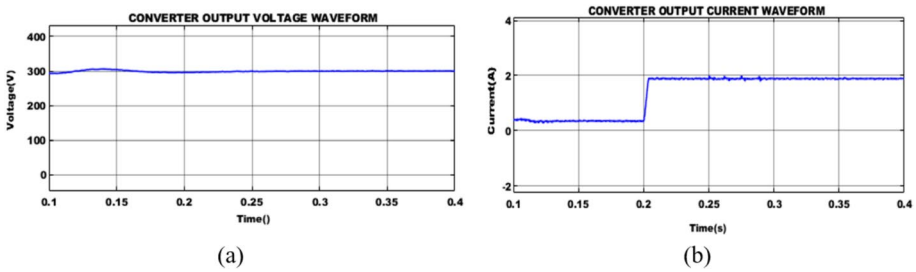

Fig. 11 Zeta-Luo converter (**a**) voltage and (**b**) current waveform

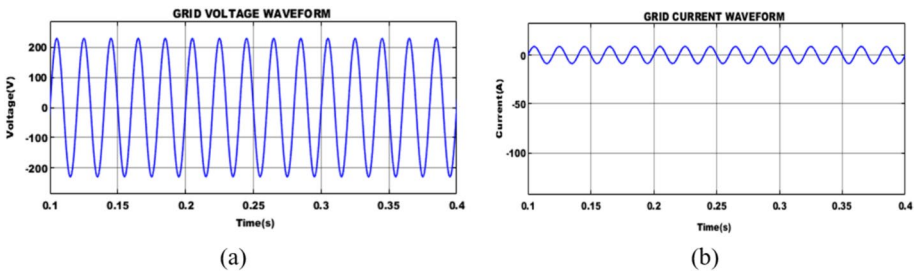

Fig. 12 Grid (**a**) voltage and (**b**) current

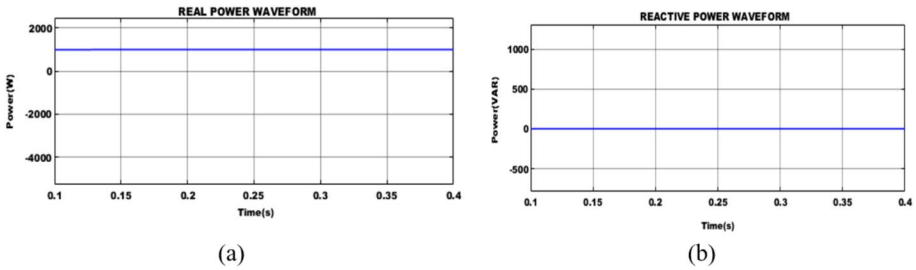

(a) (b)

Fig. 13 **a** Real and **b** reactive power waveform

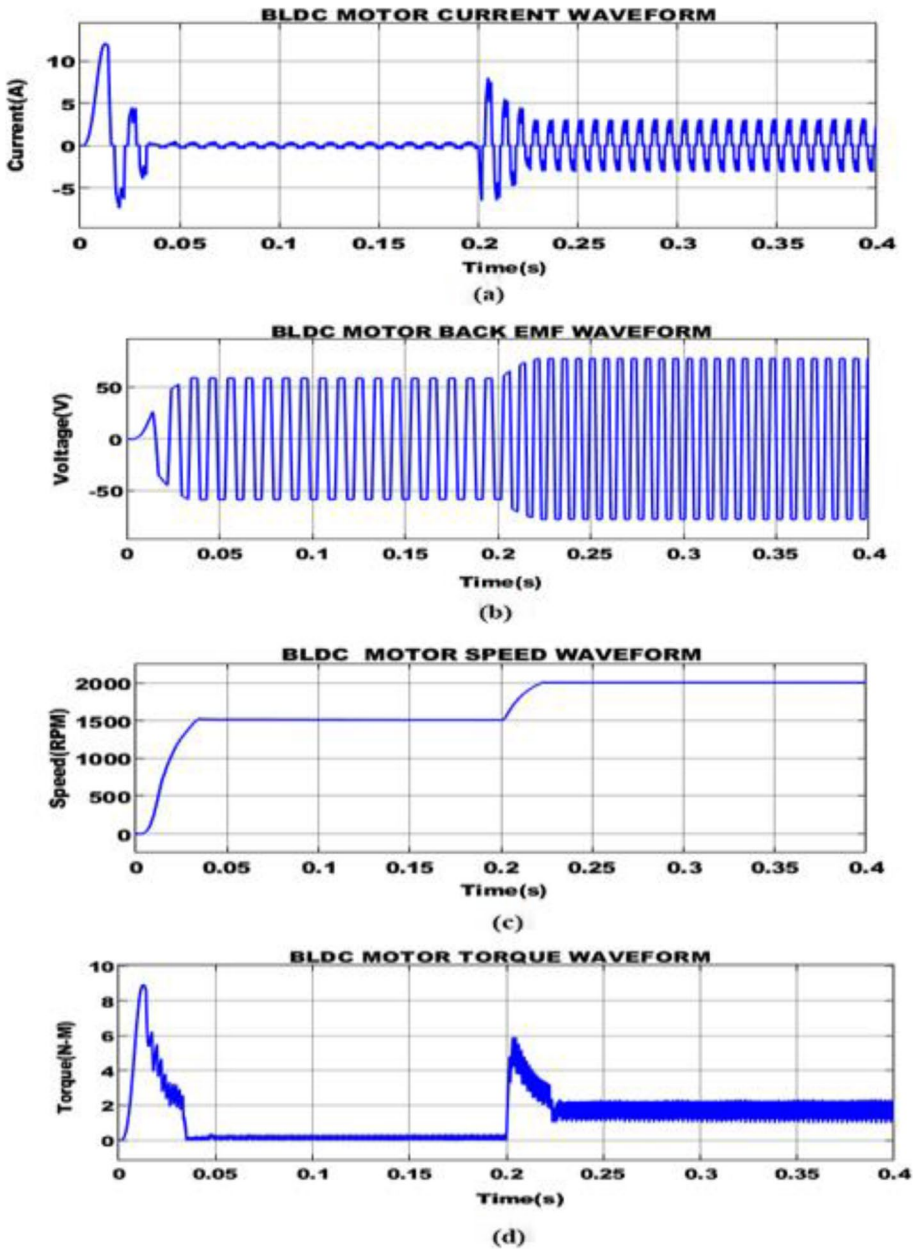

Fig. 14 BLDC motor waveforms of **a** current, **b** back EMF, **c** speed, **d** torque

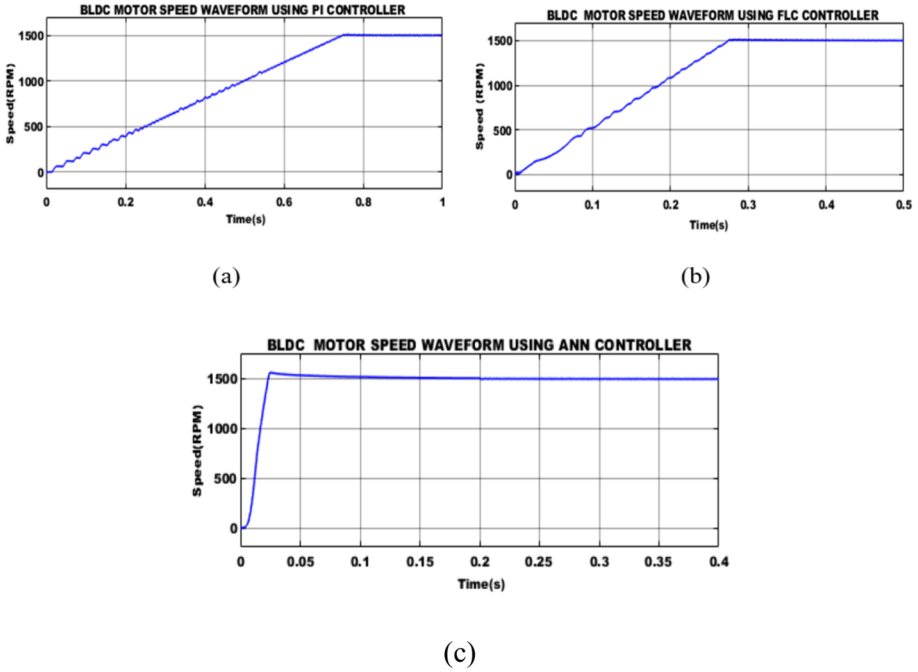

Fig. 15 BLDC motor waveforms of speed control using **a** PI controller, **b** FLC, **c** ANN controller

The motor speed is altered by varying the pulse signal's frequency, which powers the BLDC motor. This kind of speed control is often accomplished with a specialized electronic speed controller. Thus, this work uses the PI/FLC/ANN controllers for optimal speed regulation with smooth BLDC motor operation as seen in Fig. 15. From the obtained results is it proved that the ANN controller achieves a quick settling time (i.e., 0.05) when compared to other two approaches.

The amount of harmonics present in the developed system is represented in Fig. 16. It is detected that a reduced THD value of 1.43% is attained and meets the requirement of the IEEE standard.

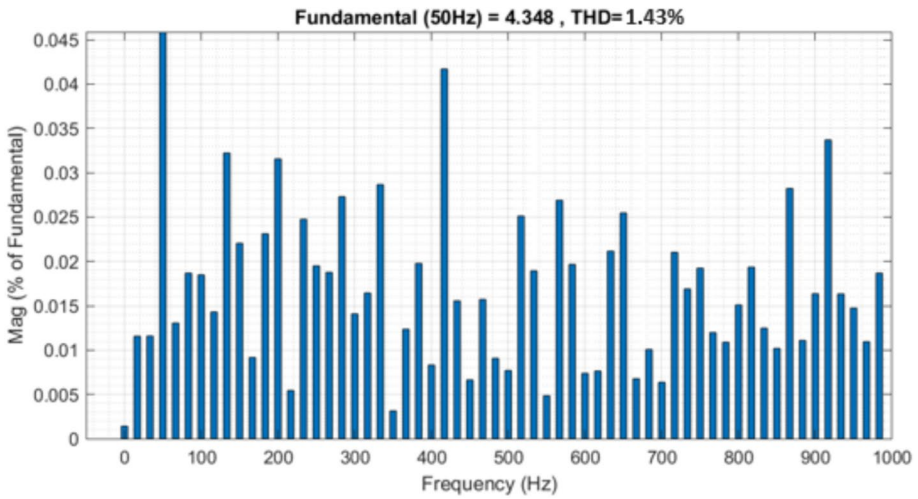

Fig. 16 THD Waveform

Table 2 Comparison of speed controllers

Controllers	Settling time
PI	0.8
FLC	0.3
ANN	0.05

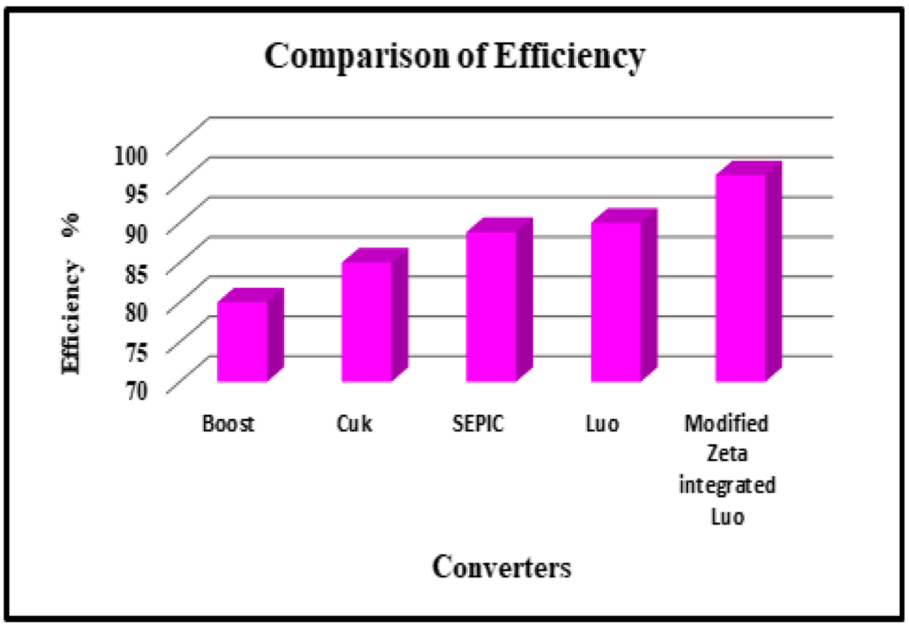

(a)

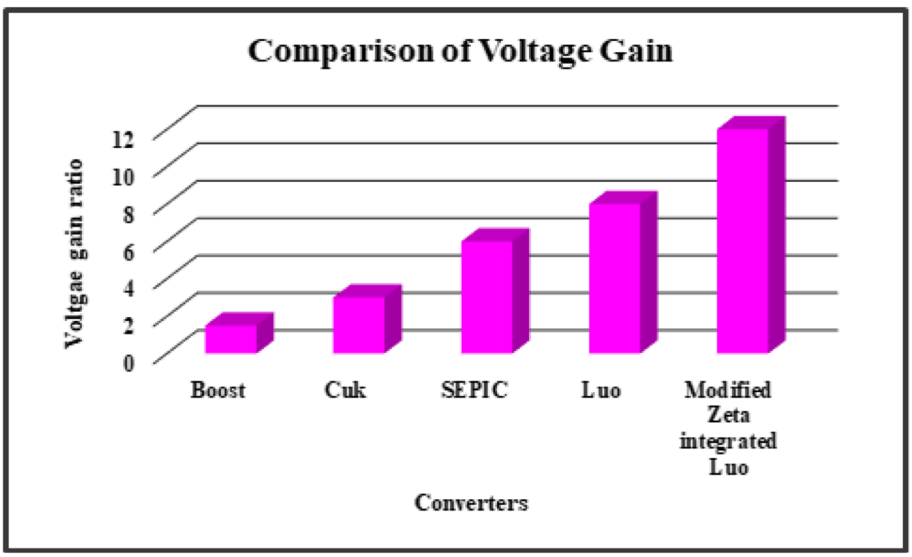

(b)

Fig. 17 Comparison of **a** efficiency, **b** voltage gain

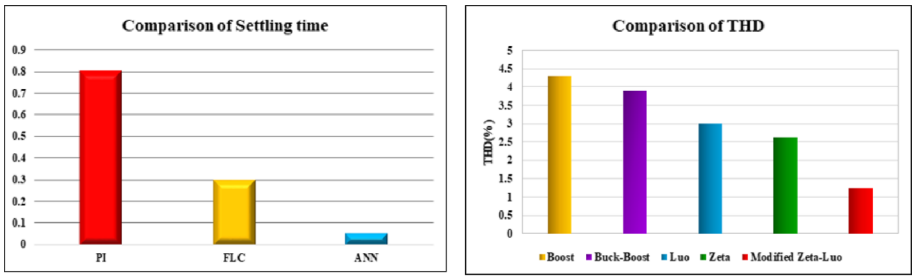

(a) (b)

Fig. 18 Comparison analysis of **a** settling time, **b** THD

From Fig. 17, the graphical representation of the proposed Modified Zeta-Luo converter efficiency and voltage gain is compared with approaches like Boost[24], Cuk[25], SEPIC[26], and Luo[27] topologies. From observation, it is clear that the proposed converter topology achieved the best efficiency of 96%, while the aforementioned converters attained, 80%, 85%, 88.82%, and 90% respectively. Similarly, a minimized voltage gain value of 1:1.5, 1:3, 1:6, and 1:8 is obtained using Boost, Cuk, SEPIC, and Luo converter approaches, while the proposed modified Zeta-Luo accomplishes a maximum voltage gain of 1:12, resulting in improved system performance.

Table 2 represents the comparison of the controller's dynamic response. The proposed converter topology and control approaches are compared with different existing approaches as shown in Fig. 18. It is noticed that a minimized THD of 1.43% with a quick settling time of 0.05s is achieved when compared to other traditional methods.

Conclusions

This paper offers a hybrid GW-GO optimization technique for a PV and MZILC-based EV charging infrastructure. PV-driven EVs have received a lot of interest due to their highlights on ecologically friendly and lower carbon emissions. A MZILC regulates a PV system's output and boosts it. Gate pulses are produced using PWM. The switching state of the MZILC is improved by the GW-GO-tuned PI controller. In this study, the GWO-PI controller is also used to guarantee a continuous, fluctuation-free voltage supply from the converter. With the aid of the proposed control approach to the MZLIC, an efficiency of 96% is attained remarkably. Due to the minimum THD value of 1.43%, harmonics have a very minimal effect. The simulation outcomes obtained from MATLAB are utilized to estimate the applicability of the designed PV-based EV system. Nevertheless, the GW-GO has poor local exploring performance, low addressing precision, and an inconsistent rate of convergence. For future work, an improved optimization algorithm can be used to achieve better results.

Abbreviations

EV	Electric vehicle
PV	Photovoltaic
BLDC	Brushless direct current
MZILC	Modified Zeta Integrated Luo Converter
PI	Proportional Integral
GW-GO	Grey Wolf–Grasshopper Optimization
SEPIC	Single-Ended Primary-Inductance Converter

GA	Genetic Algorithm
PSO	Particle Swarm Optimization
GWO	Grey Wolf Optimization
GO	Grasshopper Optimization
PWM	Pulse Width Modulation
VSI	Voltage Source Inverter
EMF	Electromagnetic Force
THD	Total harmonic distortion

Acknowledgements
The author extended their thanks to GIET University for providing the research facilities to complete the article.

Authors' contributions
The authors confirm their contribution to the paper as follows: study conception, data collection, and draft manuscript preparation: AK, BP, and RK; data analysis: RK; validation: BP and RK; conceptualization: AK; writing—review and editing: AK and BP. All authors reviewed the results and approved the final version of the manuscript.

Funding
The author(s) received no financial support for research, authorship, and/or publication of this article.

Availability of data and materials
Data sharing is not applicable to this article as no datasets were generated or analyzed during the current study.

Declarations

Competing interests
The author(s) declared no potential conflict of interest with respect to the research, authorship, and/or publication of this article.

Received: 21 October 2023 Accepted: 19 June 2024
Published online: 06 July 2024

References

1. Bhatti AR et al (2019) Optimized sizing of photovoltaic grid-connected electric vehicle charging system using particle swarm optimization. Int J Energy Res. 43(1):500–522
2. Singh B et al (2020) Implementation of solar PV-battery and diesel generator based electric vehicle charging station. IEEE Trans Ind Appl 56(4):4007–4016
3. Serpi A, Porru M (2019) Modelling and design of real-time energy management systems for fuel cell/battery electric vehicles. Energies 12(22):4260
4. Ren L, Gong C, Zhao Y (2019) An online ESR estimation method for output capacitor of boost converter. IEEE Trans Power Electron 34(10):10153–10165
5. Amir A et al (2018) Transformerless high gain boost and buck-boost DC-DC converters based on extendable switched capacitor (SC) cell for stand-alone photovoltaic system. Solar Energy 171:212–222
6. Kokare A, Patil S, Bacchav L (2017) Implementation of a highly efficient MPPT technique for a PV system using SEPIC converter. 2017 International Conference on Information, Communication, Instrumentation and Control (ICICIC). Indore: IEEE
7. Nathan K et al (2018) A new DC–DC converter for photovoltaic systems: coupled-inductors combined Cuk-SEPIC converter. IEEE Trans Energy Convers 34(1):191–201
8. Hussaian Basha CH, et al (2020) Development of cuckoo search MPPT algorithm for partially shaded solar PV SEPIC converter. Soft Computing for Problem Solving: SocProS 2018, Volume 1. Singapore: Springer Singapore
9. Verma A et al (2020) An implementation of solar PV array based multifunctional EV charger. IEEE Trans Ind Appl. Babylon 56(4):4166–4178
10. Lins AW, Krishnakumar R (2022) Tuning of PID controller for a PV-fed BLDC motor using PSO and TLBO algorithm. Appl Nanosci 13(4):2911–2934
11. Ouledali O et al (2019) Genetic algorithm tuned PI controller on PMSM direct torque control. Algerian J Renew Energy Sustain Dev 1(2):204–211
12. Thaha HS, Devaprakash R (2021) Reduction of power quality issues in micro-grid using GA tuned PI controller based DVR. J Electric Eng 21(1):8–8
13. Sultana U et al (2021) Performance analysis of real-time PSO tuned PI controller for regulating voltage and frequency in an AC microgrid. Int J Electric Comput Eng. 11(2):1068
14. Sule AH et al (2020) Grey wolf optimizer tuned PI controller for enhancing output parameters of fixed speed wind turbine. 2020 IEEE International Conference on Automatic Control and Intelligent Systems (I2CACIS). IEEE, Shah Alam, Malaysia
15. Datta U, Kalam A, Shi J (2020) Smart control of BESS in PV integrated EV charging station for reducing transformer overloading and providing battery-to-grid service. J Energy Storage 28:101224
16. Mokariya KL (2022) Solar PV based EV charging in India: the growing start-up eco system Analysis, Challenges and solutions. Adv Dyn Syst Appl 17(1):81–105
17. Yan Q, Zhang B, Kezunovic M (2018) Optimized operational cost reduction for an EV charging station integrated with battery energy storage and PV generation. IEEE Transactions on Smart Grid 10(2):2096–2106

18. Tran VT et al (2019) An efficient energy management approach for a solar-powered EV battery charging facility to support distribution grids. IEEE Transact Ind Appl 55(6):6517–6526
19. Wu Q et al (2018) Transactive real-time electric vehicle charging management for commercial buildings with PV on-site generation. IEEE Transact Smart Grid 10(5):4939–4950
20. Singh B et al (2020) Implementation of solar PV-battery and diesel generator based electric vehicle charging station. IEEE Trans Ind Appl 56(4):4007–4016
21. Radhakrishnan RKG et al (2022) An intensified marine predator algorithm (MPA) for designing a solar-powered BLDC motor used in EV systems. Sustainability 14(21):14120
22. Glenn JA, Alavandar S (2023) Hybrid optimized PI controller design for grid tied PV based electric vehicle. Intell Autom Soft Comput 36(2):1523–1545
23. Priyadarshi N et al (2020) Internet of things augmented a novel PSO-employed modified zeta converter-based photovoltaic maximum power tracking system: hardware realisation. IET Power Electron 13(13):2775–2781
24. Nejabatkhah F, Danyali S (2011) Seyed Hossein Hosseini, Mehran Sabahi, and Seyedabdolkhalegh Mozaffari Niapour, Modeling and control of a new three-input DC–DC boost converter for hybrid PV/FC/battery power system. IEEE Trans Power Electron 27(5):2309–2324
25. Galea F, Apap M, Spiteri Staines C, Cilia J (2011) Design of a high efficiency wide input range isolated Cuk Dc-Dc converter for grid connected regenerative active loads
26. Javeed P, Yadav LK, Kumar PV , Ranjit K, Swaroop S (2021) SEPIC Converter for Low Power LED Applications. In Journal of Physics: Conference Series, vol. 1818, no. 1, p. 012220. IOP Publishing
27. Sivarajeswari S, Kirubakaran D (2019) Design and development of efficient Luo converters for DC micro grid. Int J Electr Eng Educ 60, no. 1_suppl(2023):1662–1682

Publisher's Note